

Power Efficiency, Overhead, and Complexity Tradeoff in IRS-Assisted Communications – Quadratic Phase-Shift Design

Vahid Jamali, *Member, IEEE*, Marzieh Najafi, *Student Member, IEEE*, Robert Schober, *Fellow, IEEE*, and H. Vincent Poor, *Life Fellow, IEEE*

Abstract

In this paper, we focus on large intelligent reflecting surfaces (IRSs) and propose a new codebook construction method to obtain a set of predesigned phase-shift configurations for the IRS unit cells. Since the overhead for channel estimation and the complexity of online optimization for IRS-assisted communications scale with the size of the phase-shift codebook, the design of small codebooks is of high importance. We show that there exists a fundamental tradeoff between power efficiency and the size of the codebook. We first analyze this tradeoff for baseline designs that employ a linear phase-shift across the IRS. Subsequently, we show that an efficient design for small codebooks mandates higher-order phase-shift variations across the IRS. Consequently, we propose a quadratic phase-shift design, derive its coefficients as a function of the codebook size, and analyze its performance. Our simulation results show that the proposed design yields a higher power efficiency for small codebooks than the linear baseline designs.

Index Terms

Intelligent reflecting surfaces, phase-shift design, channel estimation overhead, complexity, and power efficiency.

I. INTRODUCTION

Intelligent reflecting surface- (IRS-) assisted communication is a promising emerging technology for the realization of smart wireless environments [1]. IRSs consist of a large number of

V. Jamali, M. Najafi, and R. Schober are with the Institute for Digital Communications at Friedrich-Alexander University Erlangen-Nürnberg (FAU) (e-mail: vahid.jamali@fau.de; marzieh.najafi@fau.de; robert.schober@fau.de).

H. Vincent Poor is with the Department of Electrical Engineering, Princeton University, Princeton, NJ 08544 USA (e-mail: poor@princeton.edu).

programmable sub-wavelength elements, so-called unit cells or meta atoms, that can change the properties of an impinging electromagnetic wave while reflecting it [2]. For instance, a properly designed unit-cell phase distribution across the surface allows the IRS to alter the direction of the wavefront of the reflected wave, thereby realizing the generalized Snell's law [3], [4]. However, it has been shown in the literature [5]–[7] that, for far-field applications, IRS-assisted links are effective only if the IRS is very large (e.g., comprising hundreds if not thousands of unit cells). Such large IRSs introduce various implementation challenges including large overhead for channel estimation and high complexity for online optimization.

To cope with the aforementioned challenges, the authors in [7] proposed to not directly optimize the unit-cell phase shifts, but to design a set of phase-shift configurations, referred to as transmission modes, in an offline stage, and select the best transmission mode in the online stage for a given channel realization. Similarly, in [8]–[10], the authors employed predefined phase-shift configurations based on the discrete Fourier transform (DFT) matrix for channel estimation in IRS-assisted systems. We refer to a model that characterizes the IRS in terms of the phase-shift applied by its individual unit cells as the *phase-shift model* and to a model that characterizes the IRS in terms of transmission modes as the *transmission-mode model*. In contrast to the phase-shift model, whose channel estimation overhead and online optimization complexity scale with the number of IRS unit cells, in the transmission-mode model, these quantities scale with the number of transmission modes contained in the codebook which, in principle, can be much smaller than the number of IRS unit cells. Nevertheless, the codebooks proposed in [7]–[10] may still be too big for practical implementation (e.g., the codebooks in [7] and [8]–[10] contain 100 and 400 transmission modes, respectively, for an IRS of size $10\lambda \times 10\lambda$, where λ denotes the wavelength).

Motivated by the above discussion, in this paper, we aim to design small-size but efficient phase-shift codebooks. To this end, we show that there is a fundamental tradeoff between the codebook size and the resulting transmission power efficiency such that the smaller the codebook is, the lower the power efficiency of the IRS-assisted system becomes. We first analyze this tradeoff for the baseline schemes in [7]–[10], where a *linear phase shift* across the IRS was considered. Then, we show that for small phase-shift codebooks and large IRSs, higher-order variations of the phase shifts across the IRS are needed. In particular, we propose a *quadratic phase-shift design* where the phase shifts across the IRS are quadratic functions and derive its coefficients as a function of the desired codebook size. Moreover, we derive a closed-form

approximation of the IRS response function for the proposed phase-shift design that characterizes the response of the IRS in the far-field. Furthermore, we study the tradeoff between power efficiency and codebook size for the proposed design as well as the baseline designs via computer simulations.

We note that the problem of phase-shift codebook design for IRS-assisted communication is similar to the problem of beam synthesis in millimeter-wave communications [11]–[13]. However, unlike millimeter-wave systems where the signal is known to the transmitter and the problem is to synthesize a transmission pattern along certain directions, in IRS-assisted communication, the phase distribution of the incident wave across the IRS is unknown when synthesizing the desired reflection pattern. As a result, the beam designs available in the millimeter-wave communication literature are not directly applicable to IRS phase-shift codebook design.

II. SYSTEM MODEL

In this paper, we focus on the problem of codebook design based on the transmission-mode model in [7]. Nevertheless, for completeness, we present both the phase-shift and transmission-mode models for an example IRS-assisted downlink system. This makes the relation between this work and the literature, which is mostly based on the phase-shift model, clearer.

A. Phase-shift Model

Let us consider an example downlink network consisting of a base station (BS) equipped with N_t transmit antennas serving K mobile users each equipped with N_r receive antennas. The direct links between the BS and the users may exist but are severely shadowed (e.g., by a blocking building). The downlink communication is assisted by an IRS that comprises Q reflecting unit cells. The end-to-end system model can be written as [7]

$$\mathbf{y}_k = (\mathbf{H}_{d,k} + \mathbf{H}_{r,k}\mathbf{\Omega}\mathbf{H}_i)\mathbf{x} + \mathbf{n}_k, \quad k = 1, \dots, K, \quad (1)$$

where $\mathbf{x} \in \mathbb{C}^{N_t}$, $\mathbf{y}_k \in \mathbb{C}^{N_r}$, and $\mathbf{n}_k \in \mathbb{C}^{N_r}$ denote the BS's transmit signal, the received signal at the k -th user, and the additive white Gaussian noise (AWGN) at the k -th user, respectively. Here, \mathbb{C} denotes the set of complex numbers. Moreover, $\mathbf{H}_{d,k} \in \mathbb{C}^{N_r \times N_t}$, $\mathbf{H}_i \in \mathbb{C}^{Q \times N_t}$, and $\mathbf{H}_{r,k} \in \mathbb{C}^{N_r \times Q}$ denote the BS-to-user k , BS-to-IRS, and IRS-to-user k channel matrices, respectively. Furthermore, $\mathbf{\Omega} = \text{diag}(\bar{g}e^{j\omega_1}, \dots, \bar{g}e^{j\omega_Q}) \in \mathbb{C}^{Q \times Q}$ is a diagonal matrix with diagonal entries $\bar{g}e^{j\omega_1}, \dots, \bar{g}e^{j\omega_Q}$, where ω_q is the phase-shift applied by the q -th unit cell and \bar{g} denotes the

normalized unit-cell factor. For simplicity, we assume a constant unit-cell factor $\bar{g} = \frac{4\pi A_{\text{uc}}}{\lambda^2}$, where A_{uc} is the unit-cell area; however, in general, \bar{g} may also depend on the incident and reflected angles of the waves, see [6], [7] for details.

Since Q is typically very large, the elements of $\mathbf{H}_{r,k}$ (and \mathbf{H}_i) cannot be modeled as independent random variables and the rank of $\mathbf{H}_{r,k}$ (and \mathbf{H}_i) is limited by the number of channel scatters. Adopting the low-rank channel model in [7], we decompose the channel matrices as $\mathbf{H}_i = \mathbf{A}_i \boldsymbol{\Sigma}_i \mathbf{D}_i^H$, $\mathbf{H}_{r,k} = \mathbf{A}_{r,k} \boldsymbol{\Sigma}_{r,k} \mathbf{D}_{r,k}^H$, and $\mathbf{H}_{d,k} = \mathbf{A}_{d,k} \boldsymbol{\Sigma}_{d,k} \mathbf{D}_{d,k}^H$, respectively, where the components $\{\mathbf{A}_i \in \mathbb{C}^{Q \times L_i}, \mathbf{A}_{r,k} \in \mathbb{C}^{N_r \times L_{r,k}}, \mathbf{A}_{d,k} \in \mathbb{C}^{N_r \times L_{d,k}}\}$, $\{\mathbf{D}_i \in \mathbb{C}^{N_t \times L_i}, \mathbf{D}_{r,k} \in \mathbb{C}^{Q \times L_{r,k}}, \mathbf{D}_{d,k} \in \mathbb{C}^{N_t \times L_{d,k}}\}$, and $\{\boldsymbol{\Sigma}_i \in \mathbb{C}^{L_i \times L_i}, \boldsymbol{\Sigma}_{r,k} \in \mathbb{C}^{L_{r,k} \times L_{r,k}}, \boldsymbol{\Sigma}_{d,k} \in \mathbb{C}^{L_{d,k} \times L_{d,k}}\}$ represent the receive steering matrices (corresponding to the angles-of-arrival (AoAs)), transmit steering matrices (corresponding to the angles-of-departure (AoDs)), and channel gains of the scatters, where $L_i, L_{r,k}$, and $L_{d,k}$ denote the numbers of scatters of the BS-to-IRS, IRS-to-user k , and BS-to-user k channels, respectively. Furthermore, $(\cdot)^H$ denotes the Hermitian transpose.

B. Transmission-mode Model

The transmission-mode model introduced in [7] relies on designing a predefined set of M phase-shift configurations in an offline stage which later can be selected for online transmission or channel estimation¹. Let $g_m(\boldsymbol{\Psi}_i, \boldsymbol{\Psi}_r)$ denote the normalized IRS response function for the m -th transmission mode, where $\boldsymbol{\Psi}_i = (\theta_i, \phi_i)$ and $\boldsymbol{\Psi}_r = (\theta_r, \phi_r)$ are the AoA of the incident wave and the AoD of the reflected wave, respectively, and θ and ϕ are used to denote the elevation and azimuth angles, respectively. The end-to-end system model in terms of the IRS response function can be rewritten for $k = 1, \dots, K$ as follows [7]

$$\mathbf{y}_k = \left(\mathbf{A}_{d,k} \boldsymbol{\Sigma}_{d,k} \mathbf{D}_{d,k}^H + \mathbf{A}_{r,k} \boldsymbol{\Sigma}_{r,k} \mathbf{G}_k \boldsymbol{\Sigma}_i \mathbf{D}_i^H \right) \mathbf{x} + \mathbf{n}_k, \quad (2)$$

where $\mathbf{G}_k \in \mathbb{C}^{L_{r,k} \times L_i}$ is given by

$$\mathbf{G}_k = \mathbf{D}_{r,k}^H \boldsymbol{\Omega} \mathbf{A}_i = \sum_{m=1}^M s_m \mathbf{G}_{m,k}. \quad (3)$$

Here, the element in the n_r -th row and n_i -th column of $\mathbf{G}_{m,k} = \mathbf{D}_{r,k}^H \boldsymbol{\Omega}_m \mathbf{A}_i$ is the IRS response function $g_m(\boldsymbol{\Psi}_i, \boldsymbol{\Psi}_r)$ evaluated at the n_i -th AoA of the IRS and n_r -th AoD from the IRS to the

¹To facilitate flexible optimization of the IRS, in [7], it was proposed to divide the IRS unit cells into several groups, called tiles, and to devise transmission modes for each tile. In this case, phase-shift codebooks designed in this paper can be applied for each tile.

k -th user. Moreover, Ω_m is the phase-shift matrix for the m -th transmission mode. Furthermore, $s_m \in \{0, 1\}$ is a binary variable which is equal to one if the m -th mode is selected and otherwise it is equal to zero. Since only one mode can be selected, $\sum_{m=1}^M s_m = 1$ has to hold. Throughout the paper, we assume that the IRS is a planar uniform array with Q_x (Q_y) unit cells spaced d_x (d_y) apart on the x -axis (y -axis), indexed by $n_x = 0, \dots, Q_x - 1$ ($n_y = 0, \dots, Q_y - 1$), where $Q = Q_x Q_y$ and each unit cell has an area of $A_{uc} = d_x d_y$. Moreover, for future reference, we define $A_x(\Psi_i, \Psi_r) = A_x(\Psi_i) + A_x(\Psi_r)$ and $A_y(\Psi_i, \Psi_r) = A_y(\Psi_i) + A_y(\Psi_r)$ with $A_x(\Psi) = \sin(\theta) \cos(\phi)$ and $A_y(\Psi) = \sin(\theta) \sin(\phi)$.

C. Power Efficiency, Overhead, and Complexity

In the following, we discuss the fundamental tradeoff between power efficiency, channel estimation overhead, and complexity of online IRS optimization in terms of the size of the codebook for the unit-cell phase shifts.

Power efficiency: In order to maximize the power reflected in the direction where the user is located, the IRS has to introduce an appropriate phase shift at each unit cell such that the waves propagating from all unit cells in the direction of interest add up coherently. This yields the maximum value of $|g_m(\Psi_i, \Psi_r)|$ along the user direction, which, in [7, Corollary 2], is shown to be equal to $g^{\max} = \bar{g} Q_x Q_y$. The corresponding unit-cell phase shifts depend on the AoA of the incident wave and the desired AoD in which the user is located, which are both real numbers. In order to construct a finite-size codebook, the AoA and AoD have to be discretized. Therefore, for given AoA and AoD, it is not guaranteed that there exists a transmission mode in the codebook whose value of the IRS response function is equal to g^{\max} . We characterize this reduction of received power due to the finite-size codebook by a *power efficiency* factor which is formally defined as

$$\gamma(\Psi_i, \Psi_r) = \max_{m=1, \dots, M} \left[\frac{|g_m(\Psi_i, \Psi_r)|}{\bar{g} Q_x Q_y} \right]^2. \quad (4)$$

Note that by definition, $0 \leq \gamma(\Psi_i, \Psi_r) \leq 1$ holds.

Channel estimation overhead: A common approach for codebook-based channel estimation is to have the IRS select a given phase-shift configuration from the codebook, the transmitter send pilot symbols, and the receiver estimate the end-to-end channel [8]–[10]. This procedure is repeated until the channel is estimated for all phase-shift configurations in the codebook.

Therefore, the channel estimation overhead is directly proportional to the size of the phase-shift codebook M .

Complexity of online optimization: Based on the estimated channel, the best transmission mode among those in the codebook can be selected for data transmission during online optimization. In principle, the complexity of online optimization scales linearly with the size of the codebook M ; however, efficient algorithms can be developed to further reduce the complexity, see e.g. the mode pre-selection algorithm in [7].

In summary, the larger the codebook size, the higher the power efficiency but also the larger the channel estimation overhead and the complexity of online resource allocation.

III. PHASE-SHIFT DESIGN

In this section, we focus on the channel model described in (2), introduce different phase-shift designs, and analyze the resulting IRS response functions as well as the tradeoff between power efficiency and codebook size.

A. Baseline Schemes

1) *DFT-based Design:* A common choice for the IRS unit-cell phase shifts are the columns of the DFT matrix [8]–[10]. Assuming a unit-cell spacing of $d_x = d_y = \frac{\lambda}{2}$, the phase shift applied by the (n_x, n_y) -th unit cell, denoted by ω_{n_x, n_y} , is given by

$$\mathbf{e}^{j\omega_{n_x, n_y}} = \mathbf{e}^{-\frac{j2\pi}{Q_x} m_x n_x} \times \mathbf{e}^{-\frac{j2\pi}{Q_y} m_y n_y}, \quad (5)$$

where $m_t = 0, \dots, Q_t - 1$, $t \in \{x, y\}$. Here, each pair (m_x, m_y) constitutes one element of the phase-shift codebook, i.e., the codebook size is $M = Q = Q_x Q_y$. As can be observed, (5) represents the elements of a two-dimensional DFT matrix. From (3), the IRS response function is obtained as

$$\begin{aligned} g_m(\Psi_i, \Psi_r) &= \mathbf{d}_r^H \Omega_m \mathbf{a}_i \\ &= \bar{g} \sum_{n_x=0}^{Q_x-1} \sum_{n_y=0}^{Q_y-1} \mathbf{e}^{\frac{j2\pi d_x A_x(\Psi_i, \Psi_r)}{\lambda} n_x} \mathbf{e}^{\frac{j2\pi d_y A_y(\Psi_i, \Psi_r)}{\lambda} n_y} \mathbf{e}^{j\omega_{n_x, n_y}}, \end{aligned} \quad (6)$$

where \mathbf{a}_i and \mathbf{d}_r are the steering vectors for AoA Ψ_i and AoD Ψ_r , whose elements corresponding to the (n_x, n_y) -th unit cell are given by $\mathbf{e}^{\frac{j2\pi(d_x A_x(\Psi_i) n_x + d_y A_y(\Psi_i) n_y)}{\lambda}}$ and $\mathbf{e}^{-\frac{j2\pi(d_x A_x(\Psi_r) n_x + d_y A_y(\Psi_r) n_y)}{\lambda}}$,

respectively. The following lemma gives the IRS response function $g_m(\Psi_i, \Psi_r)$ for the (m_x, m_y) -element of the codebook, denoted by $g_{(m_x, m_y)}(\Psi_i, \Psi_r)$.

Lemma 1: Given the DFT-based phase-shift design in (5) and a wave impinging on the IRS from AoA Ψ_i , the IRS has the following response function for AoD Ψ_r

$$g_{(m_x, m_y)}(\Psi_i, \Psi_r) = \bar{g} e^{-j(Q_x-1)\varpi_x} e^{-j(Q_y-1)\varpi_y} \times \frac{\sin(Q_x\varpi_x)}{\sin(\varpi_x)} \times \frac{\sin(Q_y\varpi_y)}{\sin(\varpi_y)}, \quad (7)$$

where $\varpi_t = \frac{\pi d_t A_t(\Psi_i, \Psi_r)}{\lambda} - \frac{\pi m_t}{Q_t}$, $t \in \{x, y\}$.

Proof: The proof follows the same steps as a similar proof in [7, Appendix B] and is omitted due to space constraints. ■

Corollary 1: The normalized power efficiency of the DFT-based codebook design in (5) is bounded as

$$\frac{16}{\pi^4} \stackrel{(a)}{\leq} \left[\frac{1}{Q_x Q_y \sin\left(\frac{\pi}{2Q_x}\right) \sin\left(\frac{\pi}{2Q_y}\right)} \right]^2 \leq \gamma(\Psi_i, \Psi_r) \stackrel{(b)}{\leq} 1, \quad (8)$$

where inequality (a) holds with equality as $Q_x, Q_y \rightarrow \infty$ and inequality (b) holds with equality for AoAs and AoDs for which $A_t(\Psi_i, \Psi_r) = \frac{m_t \lambda}{d_t Q_t}$, $t \in \{x, y\}$, holds.

Proof: The maximum value of $\gamma(\Psi_i, \Psi_r)$ is 1 and occurs at $\varpi_t = 0$, $t \in \{x, y\}$. Noticing the monotonically decreasing property of function $\frac{\sin(Ax)}{\sin(x)}$ around $x = 0$, the minimum value of $\gamma(\Psi_i, \Psi_r)$ occurs when ϖ_x and ϖ_y attain their maximum values which are given by $\varpi_t = \frac{\pi}{2Q_t}$, $t \in \{x, y\}$, whose substitution in (7) leads to the tighter lower bound in (8). The lower bound in (a) follows directly from $\sin(x) \leq x$, $x \geq 0$. ■

As can be seen from (8), the normalized power efficiency of the DFT-based codebook design cannot be smaller than $\frac{16}{\pi^4} \approx 0.1643$ for any AoA and AoD in the asymptotic regime of large Q_x and Q_y .

2) *Linear Phase-shift Design [7]:* The phase shift ω_{n_x, n_y} in (5) is a linear function in variables n_x and n_y with constant slopes of $\frac{2\pi m_x}{Q_x}$ and $\frac{2\pi m_y}{Q_y}$, respectively. Therefore, the codebook size is always fixed as $M = Q_x Q_y$ and the power efficiency is given in (8). Moreover, (5) is valid for a unit-cell spacing of a half wavelength. In [7], the authors considered a general linear phase shift for IRSs with general unit-cell spacing and derived the corresponding IRS response function. Next, we restate the design in [7] with a slight change of notation. In particular, the linear phase

design in [7] can be rewritten as

$$e^{j\omega_{n_x, n_y}} = e^{-\frac{j2\pi d_x \bar{\beta}_x}{M_x \lambda} m_x n_x} \times e^{-\frac{j2\pi d_y \bar{\beta}_y}{M_y \lambda} m_y n_y}, \quad (9)$$

where $m_t = 0, \dots, M_t - 1$, $t \in \{x, y\}$, $M_x M_y = M$, and $\bar{\beta}_t = \min\{4, \lambda/d_t\}$, $t \in \{x, y\}$. Here, $\bar{\beta}_t$ specifies the range of the phase-shift gradients needed in the codebook for transforming any AoA into any AoD for a unit-cell spacing of d_t , $t \in \{x, y\}$. Note that both (5) and (9) are linear phase shifts where (9) reduces to (5) for $M_x = Q_x$, $M_y = Q_y$, and $d_x = d_y = \frac{\lambda}{2}$. The IRS response function for the phase shift in (9) is identical to that given in Lemma 1 after replacing ϖ_t with $\varpi_t = \frac{\pi d_t A_t(\Psi_i, \Psi_r)}{\lambda} - \frac{\pi d_t \bar{\beta}_t m_t}{M_t \lambda}$, $t \in \{x, y\}$. Note that the resulting IRS response function is consistent with that given in [7, Proposition 2]. Next, we analyze the power efficiency of the linear design in (9) in terms of codebook size M .

Corollary 2: The normalized power efficiency of the linear phase-shift codebook design is bounded as

$$\left[\frac{\sin\left(\frac{\pi d_x \bar{\beta}_x Q_x}{2M_x \lambda}\right) \sin\left(\frac{\pi d_y \bar{\beta}_y Q_y}{2M_y \lambda}\right)}{Q_x Q_y \sin\left(\frac{\pi d_x \bar{\beta}_x}{2M_x \lambda}\right) \sin\left(\frac{\pi d_y \bar{\beta}_y}{2M_y \lambda}\right)} \right]^2 \stackrel{(a)}{\leq} \gamma(\Psi_i, \Psi_r) \stackrel{(b)}{\leq} 1, \quad (10)$$

where inequality (a) holds for $M_t \geq \frac{d_t \bar{\beta}_t Q_t}{2\lambda}$, $t \in \{x, y\}$ and inequality (b) holds with equality for AoAs and AoDs for which $A_t(\Psi_i, \Psi_r) = \frac{\bar{\beta}_t m_t}{M_t}$, $t \in \{x, y\}$. Moreover, for $M_x, M_y \rightarrow \infty$, the power efficiency approaches one for all AoAs and AoDs. Furthermore, for $M_t \leq \frac{d_t \bar{\beta}_t Q_t}{2\lambda}$, $t \in \{x, y\}$, there exist AoAs and AoDs which are not supported by the main lobe of $g_m(\Psi_i, \Psi_r)$ for any of the transmission modes in the codebook.

Proof: The proof is similar to the proof of Corollary 1 and is omitted due to space constraints. ■

Corollary 2 reveals the tradeoff between power efficiency $\gamma(\Psi_i, \Psi_r)$ and codebook size M for the linear phase-shift design in (9). In particular, the normalized power efficiency may approach one by increasing $M_x, M_y \rightarrow \infty$; however, this implies a large overhead for channel estimation and high complexity for online optimization. In fact, in practice, we are more interested in small values of M_x and M_y , where Corollary 2 states that assuming half-wavelength unit-cell spacing, M_x and M_y cannot be smaller than $\frac{Q_x}{2}$ and $\frac{Q_y}{2}$, respectively, otherwise, the power efficiency becomes very small for some AoA and AoD pairs that are supported only by the side lobes of $g_m(\Psi_i, \Psi_r)$, $\forall m$. In other words, $M > \frac{Q_x Q_y}{4}$ has to hold which is particularly limiting for large

IRSs. To cope with this issue, in the following, we propose a novel phase-shift design whereby M may assume values much smaller than $\frac{Q_x Q_y}{4}$, while the power efficiency still remains large for all AoAs and AoDs.

B. Proposed Quadratic Phase-shift Design

In the following, we first present the basic idea behind the proposed phase-shift design. Subsequently, we analyze its performance in terms of the IRS response function and the tradeoff between power efficiency and codebook size.

1) *Basic Idea Behind the Proposed Phase-shift Design:* Recall that a linear phase shift transforms a plane wave with AoA Ψ_i into another wave propagating into the direction of a certain AoD Ψ_r . However, for a finite-size codebook, we require that for each codebook element m , the IRS transforms the AoAs in a given *interval* $\Psi_i \in \mathcal{A}_{i,m}$ into the AoDs in another *interval* $\Psi_r \in \mathcal{A}_{r,m}$. In fact, for any pair $(\Psi_i, \Psi_r) \in \mathcal{A}_{i,m} \times \mathcal{A}_{r,m}$, the phase-shift function ω_{n_x, n_y} should have a component with the corresponding phase gradient for the transformation of a wave with AoA Ψ_i into a wave with AoD Ψ_r . Obviously, this is not attainable with a *linear* phase-shift design. Let us define the normalized phase-shift gradient $\frac{\partial \omega_{n_x, n_y}}{\partial n_t} \triangleq \frac{2\pi d_t}{\lambda} \beta_t(n_t)$ and the corresponding interval $\beta_t(n_t) \in \mathcal{B}_{t, m_t} \subset [0, \bar{\beta}_t)$, $t \in \{x, y\}$, for the (m_x, m_y) -th transmission mode, where $\bar{\beta}_t = \min\{4, \lambda/d_t\}$, $t \in \{x, y\}$. Since the normalized phase-shift gradient varies across the surface, i.e., $\beta_t(n_t) \in \mathcal{B}_{t, m_t}$, we require a higher-order variation of the phase shift across the IRS compared to the linear phase-shift design. Hereby, we propose the following *quadratic* phase-shift function

$$e^{j\omega_{n_x, n_y}} = e^{-\frac{j2\pi d_x}{\lambda} \left[\frac{\Delta\beta_{x, m_x}}{2Q_x} n_x^2 + \beta_{x, m_x} n_x \right]} e^{-\frac{j2\pi d_y}{\lambda} \left[\frac{\Delta\beta_{y, m_y}}{2Q_y} n_y^2 + \beta_{y, m_y} n_y \right]}, \quad (11)$$

which implies $\mathcal{B}_{t, m_t} = [\beta_{t, m_t}, \beta_{t, m_t} + \Delta\beta_{t, m_t}]$, $\forall m_t, t \in \{x, y\}$. Note that $\Delta\beta_{t, m_t} = 0$ implies a linear phase-shift design, i.e., the baseline linear phase-shift designs can be seen as special cases of the proposed quadratic design. In this paper, we focus on a uniform quantization of the phase-shift gradient leading to $\beta_{t, m_{t+1}} = \beta_{t, m_t} + \Delta\beta_t$ and $\Delta\beta_{t, m_t} = \Delta\beta_t = \frac{\bar{\beta}_t}{M_t}$, $m_t = 0, \dots, M_t - 1, t \in \{x, y\}$.

2) *IRS Response Function:* Unfortunately, substituting the quadratic phase-shift in (11) into (6) does not yield a closed-form solution for the IRS response function. To cope with this issue, we approximate the summations in (6) with the corresponding integrations which yields

an approximation of $g_{(m_x, m_y)}(\Psi_i, \Psi_r)$, denoted by $\bar{g}_{(m_x, m_y)}(\Psi_i, \Psi_r)$, i.e.,

$$\begin{aligned} \bar{g}_{(m_x, m_y)}(\Psi_i, \Psi_r) = & \tilde{g} \int_{x=0}^{L_x} \int_{y=0}^{L_y} e^{\frac{j2\pi A_x(\Psi_i, \Psi_r)}{\lambda} x} e^{\frac{j2\pi A_y(\Psi_i, \Psi_r)}{\lambda} y} \\ & \times e^{-\frac{j2\pi}{\lambda} \left[\frac{\bar{\beta}_x}{2M_x L_x} x^2 + \beta_{x, m_x} x \right]} e^{-\frac{j2\pi}{\lambda} \left[\frac{\bar{\beta}_y}{2M_y L_y} y^2 + \beta_{y, m_y} y \right]} dx dy, \end{aligned} \quad (12)$$

where $\tilde{g} = \frac{4\pi}{\lambda^2}$ and $L_t = Q_t d_t$, $t \in \{x, y\}$. The solution to the above integrals is given in the following proposition.

Proposition 1: Given the proposed quadratic phase-shift design in (11) and a wave impinging on the IRS from AoA Ψ_i , the IRS response function along AoD Ψ_r is given by

$$\begin{aligned} \bar{g}_{(m_x, m_y)}(\Psi_i, \Psi_r) = & \frac{-j\pi\tilde{g}}{4\sqrt{\vartheta_x\vartheta_y}} e^{-j\frac{\nu_x^2}{4\vartheta_x}} e^{-j\frac{\nu_y^2}{4\vartheta_y}} \\ & \times \left[\operatorname{erfi} \left(\sqrt{\frac{j}{4\vartheta_x}} \nu_x \right) - \operatorname{erfi} \left(\sqrt{\frac{j}{4\vartheta_x}} \nu_x \right) \right] \\ & \times \left[\operatorname{erfi} \left(\sqrt{\frac{j}{4\vartheta_y}} \nu_y \right) - \operatorname{erfi} \left(\sqrt{\frac{j}{4\vartheta_y}} \nu_y \right) \right], \end{aligned} \quad (13)$$

where $\vartheta_t = -\frac{\pi\bar{\beta}_t}{M_t L_t \lambda}$, $\nu_t = \frac{2\pi(A_t(\Psi_i, \Psi_r) - \beta_{t, m_t})}{\lambda}$, $\nu_t = \frac{2\pi(A_t(\Psi_i, \Psi_r) - \beta_{t, m_t} - \frac{\bar{\beta}_t}{M_t})}{\lambda}$, $t \in \{x, y\}$, and $\operatorname{erfi}(\cdot)$ is the imaginary error function.

Proof: The proof follows from the following integral identity [14]:

$$\int e^{j(\vartheta x^2 + \nu x)} dx = \sqrt{\frac{\pi}{j4\vartheta}} e^{-j\frac{\nu^2}{4\vartheta}} \operatorname{erfi} \left(\sqrt{\frac{j}{4\vartheta}} (2\vartheta x + \nu) \right) \quad (14)$$

and the simplification of the result. ■

We will show in Section IV that the analytical expression in (13) yields an accurate approximation of the IRS response function in (6) particularly around the main lobe. Although (13) explicitly characterizes the dependence of the IRS response function on the codebook size M , substituting (13) into (4) does not admit further simplification for the power efficiency. Therefore, we study the tradeoff between power efficiency and codebook size via simulations in Section IV.

C. Ideal (Unattainable) Tradeoff

Next, we derive a simple tradeoff between power efficiency and codebook size for an idealistic scenario. We consider the reflected beam pattern of the linear phase-shift design as the reference beam. First, recall that $g_m(\Psi_i, \Psi_r)$ cannot exceed $g_{\max} = \bar{g}Q_x Q_y$, which is attainable by the

reference beam only at its peak. Next, consider an ideal reflected beam, referred to as beam I_1 , which has a flat main lobe with gain g_{\max} covering $S = \frac{4\sin(\theta_r)}{Q_x Q_y}$ steradian (i.e., the maximum beamwidth for the main lobe of the reference beam along elevation angle θ_r and for all azimuth angles when Q_x and Q_y are large). The power radiated in this area is proportional to $g_{\max}^2 S = 4Q_x Q_y \sin(\theta_r)$. Now, let us construct an ideal beam I_2 by dividing the entire space over the IRS into $M_x M_y$ partitions, where $M_x \ll Q_x$ and $M_y \ll Q_y$ hold, and each subspace ($\propto \frac{2\pi}{M_x M_y}$ steradian) is supposed to be covered by one reflected beam. Following the law of conservation of energy, since beam I_2 covers an area $\frac{Q_x Q_y}{M_x M_y}$ times larger than beam I_1 , its corresponding IRS response function is $\frac{\sqrt{M_x M_y}}{\sqrt{Q_x Q_y}}$ smaller which implies $g_m(\Psi_i, \Psi_r) \leq \bar{g} \sqrt{M_x M_y Q_x Q_y}$ and $\gamma(\Psi_i, \Psi_r) \leq \frac{M_x M_y}{Q_x Q_y}$. This simple argument provides a basic intuition regarding the tradeoff between power efficiency and codebook size.

IV. SIMULATION RESULTS

In Fig. 1, we plot $|g_m(\Psi_i, \Psi_r)|^2$ in dB vs. θ_r for a) different $\Delta\beta_{i,m} = \Delta\beta = 0, 0.25, 0.5, 0.75$, b) different incident wave angles $(\theta_i, \phi_i) = (0, 0), (20^\circ, 0), (20^\circ, 180^\circ)$, and c) different IRS size $L_x = L_y = 5\lambda, 10\lambda, 20\lambda$. Fig. 1a) shows that the reflected beam becomes wider as $\Delta\beta$ increases which implies that smaller numbers of beams (i.e., smaller phase-shift codebooks) are needed to cover the entire space. On the other hand, as the beam becomes wider, the peak of the main lobe decreases which illustrates the fundamental tradeoff between power efficiency and codebook size. Note that, in practice, not only the desired reflection direction is a priori unknown but also the angle of the incident wave. Fig. 1b) shows the IRS response function for different incident angles for a fixed phase-shift configuration. This figure suggests that for the proposed phase-shift design, a change of the incident angle translates to a change of the location of the center of the reflected beam while the shape of the reflected beam is preserved. Furthermore, Fig. 1c) shows that if $\Delta\beta$ (or equivalently the codebook size and the coverage area per codebook element) is kept fixed, increasing the IRS size simply boosts $|g_m(\Psi_i, \Psi_r)|$ within the coverage area of each codebook element. Finally, Fig. 1 reveals that there is a good agreement between the IRS response function computed numerically from (6) and (11) and the approximated analytical expression in (13).

In Fig. 2, we plot $|g_m(\Psi_i, \Psi_r)|^2$ in dB vs. θ_r for a) the DFT-based phase-shift design in (5), b) the linear phase-shift design in (9), and c) the proposed quadratic phase-shift design in (11). Since we have $Q_x Q_y = 400$ unit cells, the size of the DFT-based codebook is $M = 400$, which is

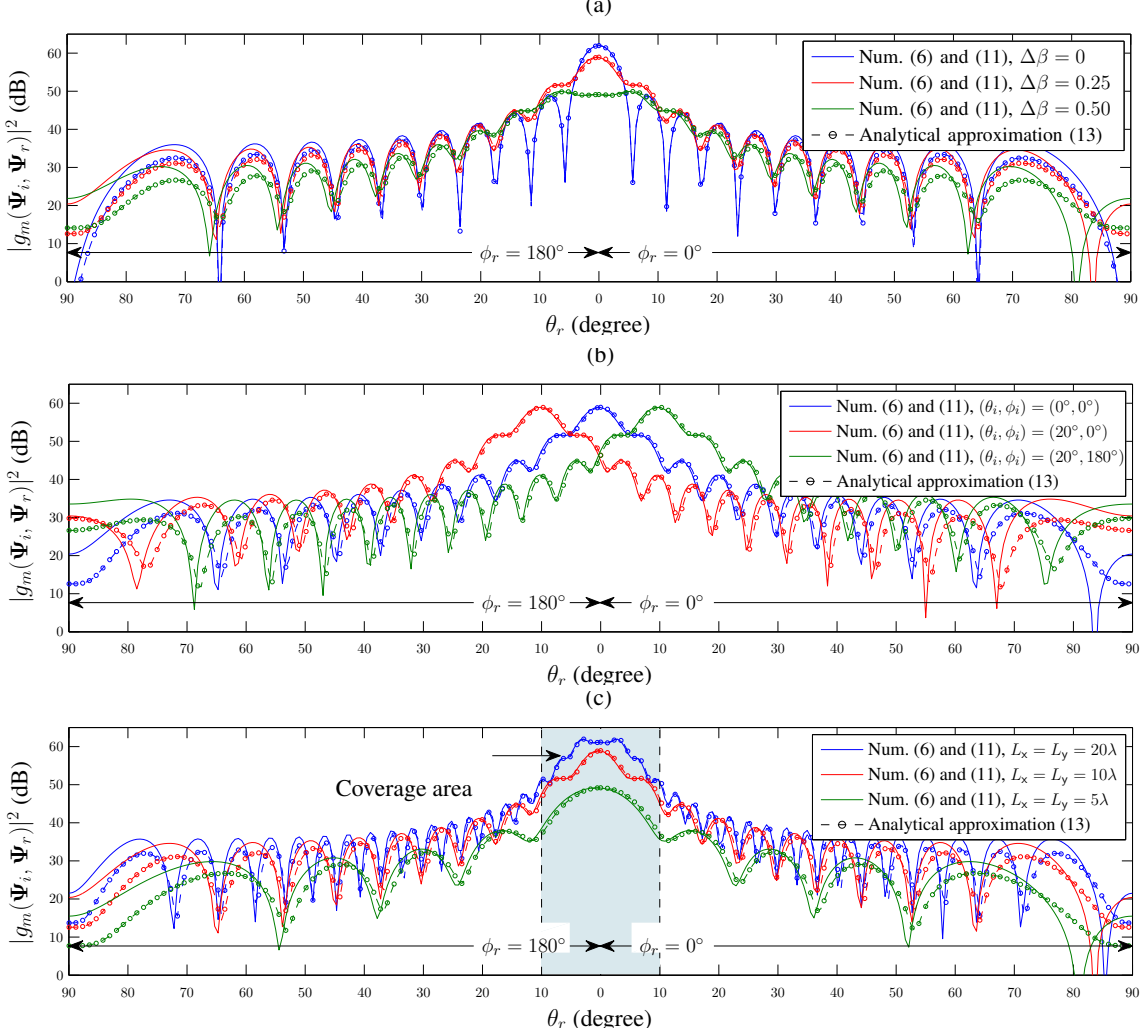


Fig. 1. $|g_m(\Psi_i, \Psi_r)|^2$ in dB vs. θ_r for $d_x = d_y = \frac{\lambda}{2}$. a) $(\theta_i, \phi_i) = (0, 0)$, $\phi_r \in \{0, \pi\}$, $L_x = L_y = 10\lambda$, and different $\Delta\beta$, b) $\phi_r \in \{0, \pi\}$, $L_x = L_y = 10\lambda$, $\Delta\beta = 0.25$, and different (θ_i, ϕ_i) , c) $(\theta_i, \phi_i) = (0, 0)$, $\phi_r \in \{0, \pi\}$, $\Delta\beta = 0.25$, and different L_x, L_y .

too large for practical implementation. For the linear design in (9), $M > \frac{Q_x Q_y}{4} = 100$ has to hold to ensure a large $\gamma(\Psi_i, \Psi_r)$, $\forall \Psi_i, \Psi_r$. In particular, we observe from Fig. 2b) that for $M = 100$, there are AoDs without coverage, i.e., $\gamma(\Psi_i, \Psi_r) = 0$. In contrast, the proposed design is able to cover the entire space with only $M = 25$ which underlines its practical relevance.

Finally, in Fig. 3, we illustrate the tradeoff between power efficiency and codebook size M . The results in Fig. 3 were obtained by averaging over 10^5 uniformly random realizations of the AoAs and AoDs for the IRS. Assuming that we are interested in ensuring a given received power, the BS's transmit power has to be proportional to $\gamma^{-1}(\Psi_i, \Psi_r)$. Therefore, $\mathbb{E}_{\Psi_i, \Psi_r} \{\gamma^{-1}(\Psi_i, \Psi_r)\}$ can be seen as a measure for the average BS transmit power, where $\mathbb{E}\{\cdot\}$ denotes expectation. In Fig. 3, we show $[\mathbb{E}_{\Psi_i, \Psi_r} \{\gamma^{-1}(\Psi_i, \Psi_r)\}]^{-1}$ vs. the codebook size which is a measure for

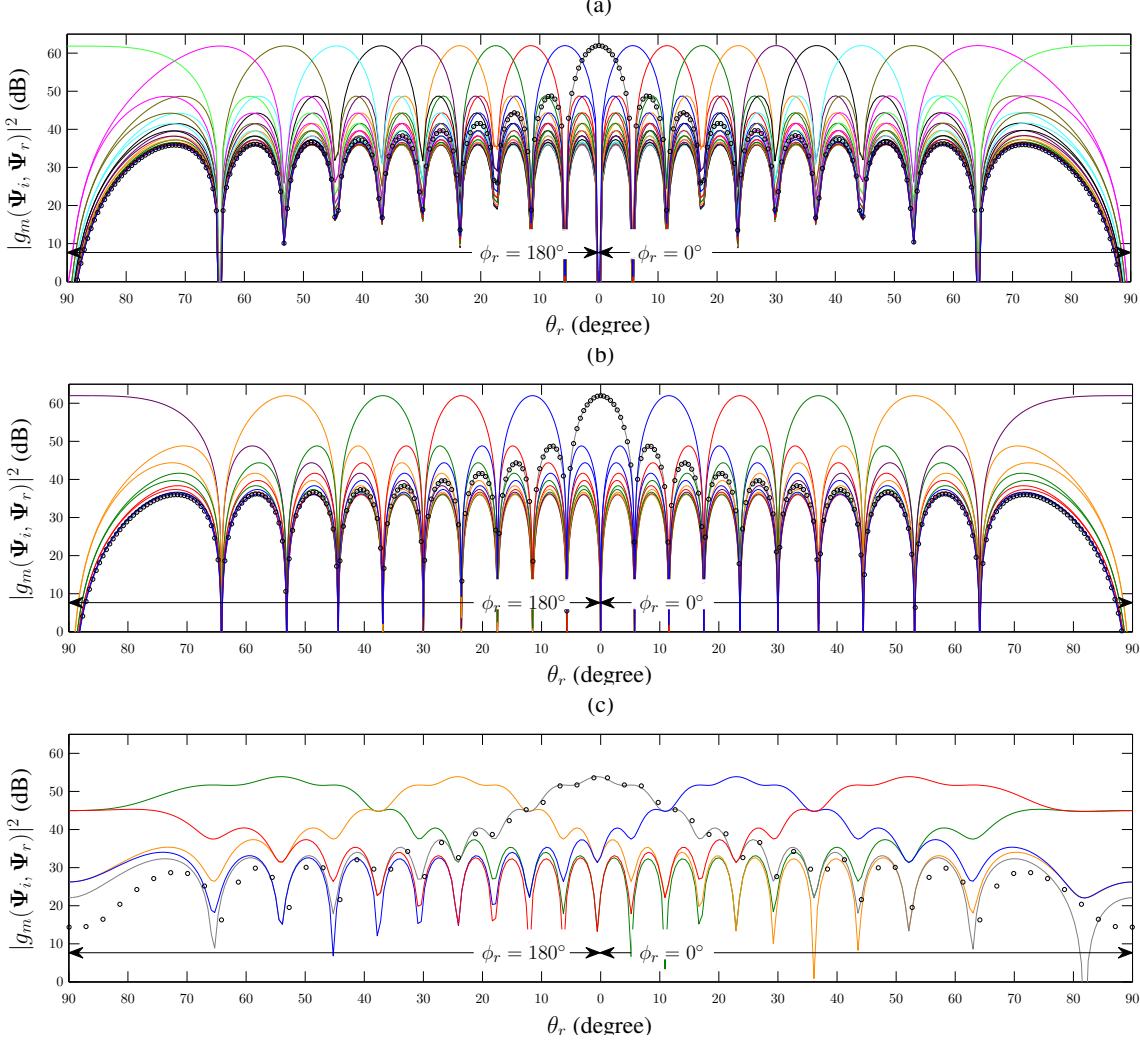


Fig. 2. $|g_m(\Psi_i, \Psi_r)|^2$ in dB vs. θ_r for $(\theta_i, \phi_i) = (0, 0)$, $\phi_r = \{0, \pi\}$, $L_x = L_y = 10\lambda$, $d_x = d_y = \frac{\lambda}{2}$. a) DFT-based phase-shift design $M = 400$, b) linear phase-shift design in [7] with $M = 100$, and c) proposed quadratic phase-shift design $M = 25$. The markers are analytical results from Lemma 1 and Proposition 1.

the channel estimation overhead and online optimization complexity. As can be seen from this figure, the DFT-based design offers a good power efficiency at the cost of a large codebook size. The linear design in [7] offers a tunable tradeoff between power efficiency and codebook size; however, the power efficiency becomes very small for small codebook sizes which is the regime of interest for many practical applications. In fact, for $M \leq 100$, there exist AoAs and AoDs which are supported only by the side lobes of $\gamma(\Psi_i, \Psi_r)$, $\forall m$, cf. Corollary 2, which is the reason for the fluctuation of the corresponding curve in Fig. 3. On the other hand, the proposed quadratic phase-shift design offers a much better tradeoff as it enables a high power efficiency even for very small codebook sizes. Furthermore, the tradeoff obtained with the proposed phase-shift design is close to the unattainable tradeoff of the ideal scenario discussed in Section III-C.

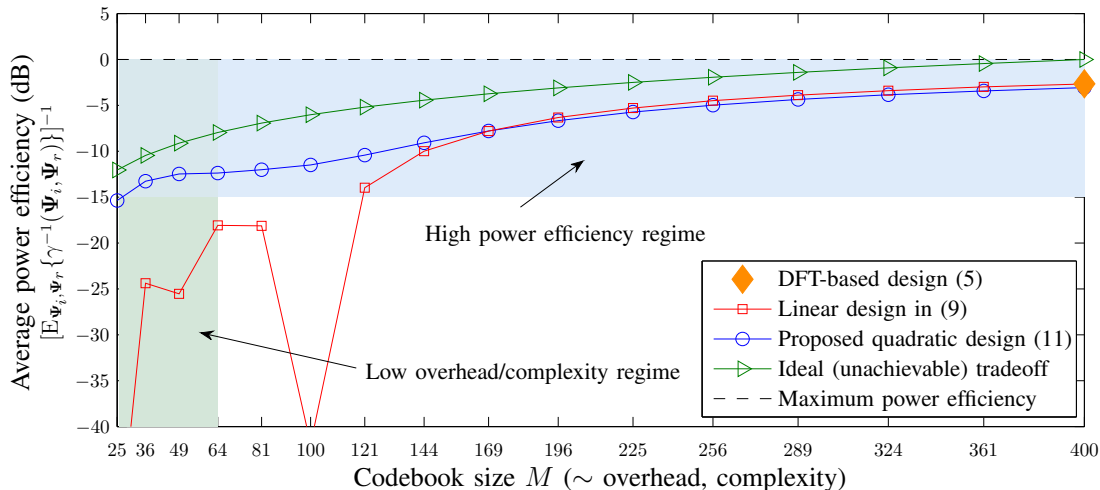


Fig. 3. Power efficiency in dB vs. phase-shift codebook size M for $L_x = L_y = 10\lambda$, $d_x = d_y = \frac{\lambda}{2}$.

REFERENCES

- [1] M. D. Renzo, et. al, "Smart radio environments empowered by AI reconfigurable meta-surfaces: An idea whose time has come," *EURASIP J. Wireless Commun. Netw.*, vol. 129, May 2019.
- [2] V. Jamali, A. Tulino, G. Fischer, R. Müller, and R. Schober, "Intelligent reflecting and transmitting surface aided millimeter wave massive MIMO," *arXiv preprint arXiv:1902.07670*, 2019.
- [3] N. M. Estakhri and A. Alù, "Wave-front transformation with gradient metasurfaces," *Physical Review X*, vol. 6, no. 4, p. 041008, 2016.
- [4] M. Najafi, B. Schmauss, and R. Schober, "Intelligent reconfigurable reflecting surfaces for free space optical communications," *under revision for IEEE Trans. Commun.*, 2020. [Online]. Available: <https://arxiv.org/abs/2005.04499>
- [5] E. Björnson and L. Sanguinetti, "Power scaling laws and near-field behaviors of massive MIMO and intelligent reflecting surfaces," *arXiv preprint arXiv:2002.04960*, 2020.
- [6] M. Di Renzo, F. H. Danufane, X. Xi, J. de Rosny, and S. Tretyakov, "Analytical modeling of the path-loss for reconfigurable intelligent surfaces—Anomalous mirror or scatterer?" *arXiv preprint arXiv:2001.10862*, 2020.
- [7] M. Najafi, V. Jamali, R. Schober, and V. Poor, "Physical modeling and scalable optimization of large intelligent reflecting surfaces," *under revision for IEEE Trans. Commun.*, 2020. [Online]. Available: <https://arxiv.org/abs/2004.12957>
- [8] B. Zheng and R. Zhang, "Intelligent reflecting surface-enhanced OFDM: Channel estimation and reflection optimization," *IEEE Wireless Commun. Lett.*, vol. 9, no. 4, pp. 518–522, Apr. 2019.
- [9] C. You, B. Zheng, and R. Zhang, "Channel estimation and passive beamforming for intelligent reflecting surface: Discrete phase shift and progressive refinement," *IEEE J. Select. Areas in Commun.*, 2020.
- [10] H. Alwazani *et al.*, "Intelligent reflecting surface-assisted multi-user MISO communication: Channel estimation and beamforming design," *IEEE Open J. Commun. Society*, vol. 1, pp. 661–680, Jun. 2020.
- [11] P. Cao, J. S. Thompson, and H. Haas, "Constant modulus shaped beam synthesis via convex relaxation," *IEEE Antenna Wireless Prop. Lett.*, vol. 16, pp. 617–620, Mar. 2017.
- [12] J. Palacios, D. De Donno, and J. Widmer, "Lightweight and effective sector beam pattern synthesis with uniform linear antenna arrays," *IEEE Antenna Wireless Prop. Lett.*, vol. 16, pp. 605–608, Mar. 2017.

- [13] D. De Donno, J. Palacios, and J. Widmer, "Millimeter-wave beam training acceleration through low-complexity hybrid transceivers," *IEEE Trans. Wireless Commun.*, vol. 16, no. 6, pp. 3646–3660, Jun. 2017.
- [14] Wolfram—Alpha, "Wolfram Alpha LLC," Aug. 7 2020. [Online]. Available: https://www.wolframalpha.com/input/?i=integral+exp%28i*%28A*x%5E2%2BB*x%29%29